Draft version January 17, 2007
Preprint typeset using LaTeX style emulateapj v. 11/26/04

CORONAL "WAVE": MAGNETIC FOOTPRINT OF A CME?

Gemma D.R. Attrill[1], Louise K. Harra[1], Lidia van Driel-Gesztelyi[1,2,3] and Pascal Démoulin[2]

Draft version January 17, 2007

ABSTRACT

We investigate the properties of two "classical" EIT coronal waves. The two source regions of the associated CMEs possess opposite helicities and the coronal waves display rotations in opposite senses. We observe deep core dimmings near the flare site and also widespread diffuse dimming, accompanying the expansion of the EIT wave. We also report a new property of these EIT waves, namely that they display dual brightenings: persistent ones at the outermost edge of the core dimming regions and simultaneously diffuse brightenings constituting the leading edge of the coronal wave, surrounding the expanding diffuse dimmings. We show that such behaviour is consistent with a diffuse EIT wave being the magnetic footprint of a CME. We propose a new mechanism where driven magnetic reconnections between the skirt of the expanding CME magnetic field and quiet-Sun magnetic loops generate the observed bright diffuse front. The dual brightenings and the widespread diffuse dimming are identified as innate characteristics of this process.

Subject headings: MHD — Sun: activity — Sun: filaments — coronal wave — Sun: magnetic fields

1. INTRODUCTION

The first observations of large-scale transient coronal waves were made by SOHO/EIT (Delaboudiniére et al. 1995). Since the mean EIT wave speed (Klassen et al. 2000) exceeds the sound speed in the corona and the intrinsic characteristics of a fast-mode shock are capable of producing brightening in EUV images, authors such as Wang (2000), Ofman & Thompson (2002), Warmuth et al. (2004b) (and references therein) and Ballai, Erdélyi & Pintér (2005), endorse the interpretation of these phenomena as fast-mode waves. When EIT waves were first observed, Uchida (1968) suggested that they could be the flare-induced coronal counterpart of the hydrodynamic chromospheric Moreton fast shock wave (Moreton 1960). More recently however, statistical studies (Biesecker et al. 2002; Cliver et al. 2005a) have shown EIT waves to be more closely associated with CMEs than with flares. Chen (2006) concluded that it is unlikely that pressure pulses from flares are responsible for generating EIT waves. The interpretation of these waves as flare-induced or piston-driven by the CME (e.g. Chen et al. 2002), thus remains open for debate.

It has also been suggested that EIT waves are not real waves at all. Rather, rearrangement of the magnetic structure during eruption of a CME may cause electric currents and pressure increases, observed as brightenings (Delannée & Aulanier 1999; Delannée 2000). Manoharan et al. (1996) show remote soft X-ray brightenings linked to a CME that developed into dimmings. Balasubramaniam et al. (2005) present a study of sequential chromospheric brightenings forming a large-scale propagating disturbance. Both authors speculate that the brightenings represent footpoints of overlying and nested coronal loop field lines respectively, energised by magnetic reconnection as the fields are progressively torn away during a CME.

Since 1996, several hundred EIT waves have been observed and a picture is emerging of two distinct types of EIT wave: those with a sharp bright front "S-waves" (Biesecker et al. 2002), often high velocity (> several hundred km s^{-1}) and sometimes co-spatial with a Moreton wave (Thompson et al. 2000a; Warmuth et al. 2001; Khan & Aurass 2002) and those with a more diffuse bright front (e.g. Thompson et al. 1998, 1999). By far the majority belong to the latter category (although this may be an artifact of the relatively low cadence of EIT). Harra & Sterling (2003) and Zhukov & Auchére (2004) suggest that different physical mechanisms may be responsible for the two different waves, whilst Thompson et al. (2000a) suggest the two types may reflect a strongly driven and then freely propagating stage of one common driver. Warmuth et al. (2004a,b) and Cliver et al. (2005b) argue for a unified view embracing many of the different types of large-scale solar disturbances (favouring flare and CME driven, respectively), including Moreton, EIT, He I 10830 Å , soft X-ray waves and type II radio bursts.

Coronal dimming has also been associated with front-side CMEs (Thompson et al. 2000b). There appear to be two types: deep core dimmings, sometimes shown to correspond to the footpoints of the erupted flux rope (e.g. Webb et al. 2000) and a more widespread dimming, observed to correspond well to the spatial extent of CMEs detected in coronagraph data (Thompson et al. 2000b). For the well-known 1997 May 12 event, Zhukov & Auchére (2004) estimate that $\sim 50\%$ of the CME mass comes from the deep core dimmings and the remaining 50% from the more widespread dimmings.

In this work, we focus on the diffuse EIT coronal wavefronts and their associated dimmings. Of particular interest is the new analysis of the 1997 May 12 EIT wave by Podladchikova & Berghmans (2005), showing that the wave displays a rotation as it propagates.

[1] University College London, Mullard Space Science Laboratory, Holmbury St. Mary, Surrey, RH5 6NT, U.K; gdra@mssl.ucl.ac.uk, lkh@mssl.ucl.ac.uk, lvdg@mssl.ucl.ac.uk.
[2] Observatoire de Paris, LESIA, UMR 8109 (CNRS), F-92195 Meudon-Principal Cedex, France; lidia.vandriel@obspm.fr, pascal.demoulin@obspm.fr.
[3] Konkoly Observatory, P.O. Box 67, H-1525 Budapest, Hungary; vandriel@konkoly.hu.

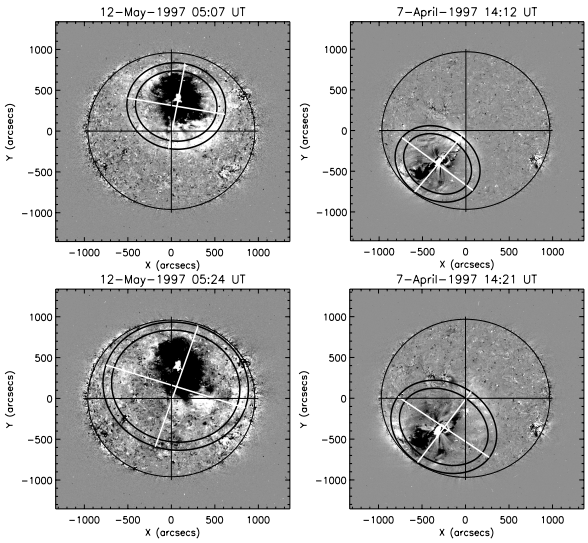

FIG. 1.— Successive base difference images for 1997 May 12 (*left*) and 1997 April 7 (*right*) coronal wave events. The bright fronts are overlaid with concentric *black ellipses*.

2. EUV OBSERVATIONS AND DATA ANALYSIS

2.1. *Intensity analysis of the coronal wavefronts*

We present two events that posess the "classical", semi-isotropic diffuse bright front: the extensively studied event on 1997 May 12 (Thompson et al. 1998; Podladchikova & Berghmans 2005) and the event on 1997 April 7 (Thompson et al. 1999). Both events are associated with partial filament eruptions, flares and front-side halo CMEs. The May event occurs in the northern hemisphere from AR 8038, which exhibits a pre-eruption reverse "S" sigmoidal structure, often cited as an indicator of negative helicity (Leamon, Canfield & Pevtsov 2002). The April event is associated with AR 8027, located in the southern hemisphere, where a pre-eruption forward "S" (positive helicity) sigmoidal structure is visible.

The coronal wave of each event is captured in two successive EIT 195 Å base difference images (Figure 1). We use running difference images to identify short-term transient features, but base difference images (corrected for solar rotation) to analyse intensity since running difference images can show false brightenings and dimmings (e.g. Chertok & Grechnev 2005). The base images are at 04:50 UT for May 12 and 14:00 UT for April 7.

After Podladchikova & Berghmans (2005), we analyse the intensity of the coronal wavefront as a function of azimuthal angle around the wavefront. We assume an isotropic, circular expansion around an epi-centre. We account for line-of-sight (LOS) projection effects (e.g. DeForest 2004). As a result, a circular EIT wave is observed as an ellipse in projection. The ellipse characteristics are defined by the initial location of the eruption (in particular θ, the angle at the centre of the solar sphere, between the observer's LOS and the initial epi-centre of the eruption on the solar surface) and by the angular radius, δ, of the EIT wave (the half-cone angle subtended at the centre of the solar sphere).

We sum the intensity, I, of the ring defined by the black ellipses shown in Figure 1. By changing δ and systematically shifting the centre of the ellipse +/- 10 arcsecs about the initial epi-centre (taken as the location of the associated flare: May 12, Thompson et al. 1998; April 7, Aurass, Vršnak & Mann 2002), we objectively find the best values for the centre (so the ellipticity and the axis) and δ of the ellipse which capture most of the coronal wave intensity.

The rings defined by the black ellipses (overlaid on the bright fronts) in Figure 1 are not concentric. The projection effect implies that as the EIT wave progresses (as δ increases), the centre of the projected coronal wave moves toward the disk centre. Thus a shift of the coronal wave centre is expected in the projected images, and its distance from the disk centre is given by: $R_\odot \sin\theta \cos\delta$.

Taking δ from the fitted black ellipses and measuring the distance from the disk centre to the centre of the ellipse, we compute θ for each of the ellipses. We compare this fitted θ with the θ defined by the location of the flare. The two θs correspond relatively well, with the exception of 05:24 UT on May 12 where they differ by 10°. We attribute this difference to the distorting effect of the north polar coronal hole (Attrill et al. 2006), artificially altering the centre of the ellipse and the ellipticity. The April 7 event encounters no such distortion and the two θs agree to $\pm$ 2°. Thus it is a valid assumption that the de-projected EIT waves are concentric circles, approximately centered on the flare location.

Since the projection of the wave changes as it propagates over the solar disk, using the projected azimuthal angle can induce a fake rotation. To avoid this, we plot the intensity as a function of the de-projected azimuthal angle (in the plane perpendicular to the local vertical at the epi-centre of the wave, i.e. the azimuthal angle around the real circle). We use the axes of the ellipse as a reference for the azimuthal angle. The tilt of the minor axis from the main solar axes is defined solely by the epi-centre of the coronal wave on the disk and therefore remains constant throughout the expansion of each event, as does the ellipticity ($= \cos\theta$).

The diffuse brightenings are highly suseptible to noise. To reduce the noise, we average the data in both the radial direction, from the inner to the outer ellipse and in the azimuthal direction, using boxcar smoothing with a smoothing kernel of 11°. The mean intensity of the ring is then plotted as a function of the de-projected azimuthal angle for the two sucessive images where the coronal wave is visible (Figure 2). The vertical lines mark the weighted mean for each peak. The lower panels show the weighted mean of the intensity of the later coronal wavefront peak(s) phase-shifted to match those of the earlier coronal wavefront peak(s). We present our interpretation of this phase shift in Section 3.1.

2.2. *Radial features of the coronal waves*

Intensity profiles (Figure 3) made in a radial direction from the centre of the disturbance reveal the diffuse brightening to be consistently concentrated in two places; at the outermost edge of the deep dimming regions and simultaneously at the leading edge of the expanding wavefront. The brightenings show an increase in intensity by a factor 8 (May 12) and factor 6 (April 7) of the respective quiet Sun intensities.

The base difference images in Figure 3 also show widespread diffuse dimmings associated with each event (*regions bounded by black dashed lines*) and persistent brightenings are marked by *white arrows* at the edge of the deep dimmings. In contrast to the deep, core dim-

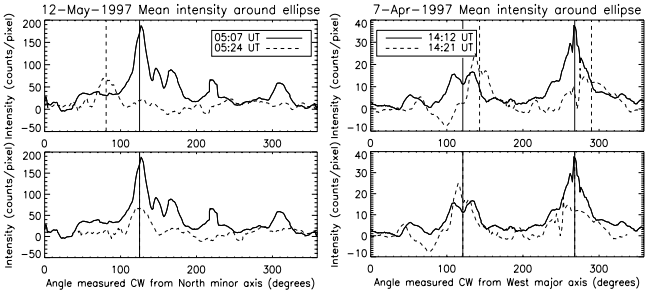

FIG. 2.— Mean intensity of the ring defined by the black ellipses shown in Figure 1 as a function of the de-projected azimuthal angle. *Left* and *right panels* show data from the May 12 and April 7 events respectively. The *vertical lines* mark the weighted mean for each peak. The *lower panels* show the weighted mean of the later peak(s) phase-shifted to match those of the earlier peak(s).

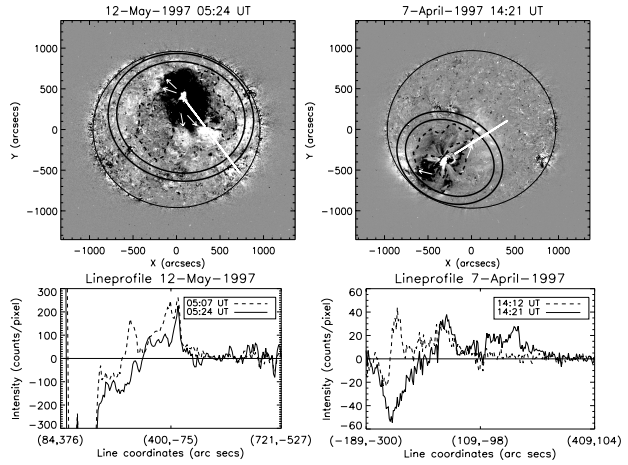

FIG. 3.— *Top panels* show the later base difference image for the May 12 (*left*) and April 7 (*right*) events, with the *fitted black ellipses* (Figure 1) marking the location of the expanded coronal wavefront. Concentrations of intensity are located at the edge of the deep core dimming regions (*white arrows*) and simultaneously at the leading edge of the coronal wave in both cases. The *black dashed lines* enclose regions of widespread diffuse dimming. The *lower panels* show intensity profiles made along the *straight white lines* in the *top panels*. The *dashed (solid) lines* show the intensity profiles from the earlier (later) base difference heliograms.

mings seen in the intensity profiles of Figure 3 (also see Attrill et al. 2006; Zarro et al. 1999), the diffuse dimmings are weak and extend to large distances from the core dimmings. They rapidly propagate across the solar disk, behind the leading bright front.

3. INTERPRETATION

3.1. *Phase shift of intensity as a function of azimuthal angle*

Figure 2 shows a phase shift of the mean intensity for each event, being 44° anti-clockwise (ACW) for the May 12 peak (confirming the result obtained by Podladchikova & Berghmans 2005) and 22° clockwise (CW) for both peaks of the April 7 event.

From the standard flare model (e.g. Shibata et al. 1995) the erupting filament/flux rope forms the core of the CME and is the driver of the "skirt" of the CME. If this skirt corresponds to the coronal wavefront, then one expects the behaviour of the coronal wave to be linked with that of the filament. Webb et al. (2000) describe an ACW rotation of the partially erupting filament, just prior to the coronal wave event on May 12. We therefore

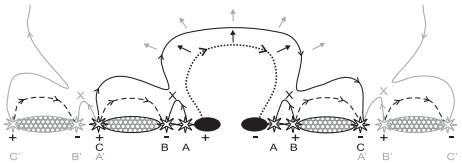

FIG. 4.— Cartoon illustrating the magnetic reconnection model proposed to generate the bright, diffuse coronal "wave" front, with the observed dual brightenings and two types of dimmings. The expanding CME (*dotted line*) reconnects with favourably orientated quiet Sun magnetic loops (*dashed lines*), displacing the footpoints of the expanding CME (*solid line*). The "**X**"s mark regions where magnetic reconnection occurs. The *dotted/dashed lines* show the pre-eruption magnetic structures, the *black (grey) solid lines* show the result of the first (subsequent) reconnections.

interpret the phase-shift of the EIT bright front (Figure 2) as an indication that the rotation of the CME magnetic structure continued following the initial rotation of the erupting core. Although a CW rotation is suggested for the April 7 case (Green et al. 2007), it is more difficult to confidently analyse the Hα data because projection effects become important. In addition, the source region helicity is different for each event (Section 2.1).

If the helicity of the source region determines the sense of the subsequent rotation of the coronal wavefront (identified above as the "skirt" of the CME), then this poses a challenge to the standard MHD "blast wave" interpretation: why should a flare-induced blast wave take account of the helicity of the CME source region? Our results suggest that the EIT coronal wave is driven by the erupting magnetic configuration, rather than by a blast wave.

3.2. *Our model*

We therefore propose a new mechanism where the bright fronts that constitute the diffuse EIT "wavefront" are due to heating caused by the expanding CME magnetic field being thrust into and reconnecting with favorably orientated "open" or "closed" magnetic structures. Since the two events we analyse occurred in a quiet-Sun (QS) environment, we focus here on interaction with QS loops and scattered "open" field lines.

With reference to Figure 4, the expanding CME structure (*dotted line*) reconnects with surrounding favourably orientated QS loops (*dashed lines*). These reconnections produce brightenings at points **A**, **B** and **C**, as a result of chromospheric evaporation (this is a lower energy version of the physics which happens in flares). The flux rope is assumed to expand in all directions at about the same rate and to be anchored in the deep dimming regions. It is the low part of the flux rope (near the footpoints) which is able to reconnect the most with low-lying QS loops, hence the concentrations in intensity (Figure 2). Brightenings **A** may be mixed with the deep dimming or be spatially unresolvable from brightenings **B**, so forming the brightening at the edge of the deep dimmings, whilst brightenings **C** are responsible for the leading edge bright wavefront. Together these brightenings make up the diffuse dual-brightening coronal wave (Figure 3).

The brightening from each reconnected loop will progressively disappear on the time-scale defined by the thermal cooling of the plasma. However, an almost stationary brightening located at the edge of the deep dimmings (*black regions*) persists (Figure 3), because the expanding core magnetic structure continues to drive re-

connections with the low-lying loops there.

The reconnection can also create longer field lines (*solid lines*, Figure 4) and therefore a larger volume within the expanding CME cavity (brightenings **C** are displaced CME footpoints). Plasma previously contained by the closed QS loops (*dashed lines*) is suddenly released into a much larger volume. As a result, we observe diffuse dimming (*hashed regions*), that can develop only after the brightenings have occured. Reconnection with "open" field lines would only create brightenings **A**,**B**, and would not contribute to the appearance of the diffuse dimmings. Given the large spatial distribution of the diffuse dimmings for these events (Figure 3), we believe that reconnection with QS loops is a more important process in the studied two cases.

After the first reconnections, the continuing expansion drives the dual-brightening signatures of the subsequent reconnections. The diffuse leading edge bright front therefore appears to propagate, being formed by successive reconnections with QS loops progressively further away, forming many brightenings **A'**, **B'**, **C'**. This implies a progression of the diffuse "EIT wave" front by steps, with a global average motion defined by the expansion of the CME core. Our model does not require a pre-existing giant bipolar arcade to span the diameter of the observed coronal wave (as in Chen et al. 2002), since this is naturally created by the displacement of the expanding CME footpoints, through the successive small-scale reconnection events between the erupting magnetic configuration and QS loops.

4. CONCLUSIONS

The behaviour of the diffuse coronal bright front appears to be linked to the helicity of the source region and to the sense of rotation of the erupting flux rope/filament. The apparently discerning rotation of the bright fronts poses an interesting challenge to the interpretation of these phenomena as flare induced blast-waves.

We propose that the diffuse EIT coronal bright fronts are due to driven magnetic reconnections between the skirt of the expanding CME magnetic field and favourably orientated QS magnetic loops. Such a mechanism appears to explain the dual bright fronts and the widespread diffuse dimming, while the deep dimmings correspond to the expansion of the core footpoints of the erupting flux rope.

With the above model, we suggest that diffuse EIT bright fronts do not "stop" at or "avoid" active regions or coronal holes (Thompson et al. 1998, 1999). Rather, they slow down substantially, and they undergo many magnetic reconnections if the skirt of the CME encounters a concentrated region of favourably orientated magnetic field. Or conversely, if the skirt encounters a region of unfavourably orientated magnetic field, then the conditions required for magnetic reconnection will not exist, and the bright front will vanish.

The higher time-cadence of data from *Hinode*, STEREO and SDO should allow a greater statistical analysis of the relationship between the helicity of the event source region, the sense of rotation of the erupting filament/flux rope and the behaviour displayed by the expanding coronal bright front.

We thank the referee for helpful comments and I. V. Alexeev for useful discussions. G.D.R.A is grateful to PPARC for support. L.K.H. acknowledges the Leverhulme Trust for the award of a Philip Leverhulme prize. L.v.D.G acknowledges the Hungarian government grant OTKA 048961.

REFERENCES

Attrill G., Nakwacki, N., Harra, L.K., van Driel-Gesztelyi, L., Mandrini, C.H., Dasso, S. & Wang, J. 2006, Sol. Phys., 238, 117
Aurass H., Vršnak, B., & Mann, G. 2002, A&A, 384, 273
Balasubramaniam K. S., Pevtsov, A. A., Neidig, D. F., Cliver, E. W., Thompson, B. J., Young, C. A., Martin, S. F. & Kiplinger, A. 2005, ApJ, 630, 1160
Ballai, I., Erdélyi, R., & Pintér, B. 2005, ApJ, 633, L145
Biesecker, D. A., Myers, D. C., Thompson, B. J., Hammer, D. M. & Vourlidas, A. 2002, ApJ, 569, 1009
Chen, P. F., Wu, S. T., Shibata, K., & Fang, C. 2002, ApJ, 572, 99
Chen P. F. 2006, ApJ, 641, L153
Chertok, I. M., & Grechnev, V. V. 2005, Sol. Phys., 229, 95
Cliver, E. W., Laurenza, M., Storini, M., and Thompson, B. J. 2005a, ApJ, 631, 604
Cliver, E. W., Nitta, N. V., Thompson, B. J., and Zhang, J. 2005b, Sol. Phys., 225, 105
DeForest, C. E. 2004, Sol. Phys., 219, 3
Delaboudiniére, J. P., et al. 1995, Sol. Phys., 162, 291
Delannée, C. 2000, ApJ, 545, 512
Delannée, C. & Aulanier, G. 1999, Sol. Phys., 190, 107
Green, L. M., Kliem, B., Török, T., van Driel-Gesztelyi, L., & Attrill, G. 2007, Sol. Phys., submitted
Harra, L. K. & Sterling, A. C. 2003, ApJ, 587, 429
Khan, J. I. & Aurass, H. 2002, A&A, 383, 1018
Klassen, A., Aurass, H., Mann, G., & Thompson, B. J. 2000, A&AS, 141, 357
Leamon, R. J., Canfield, R. C., & Pevtsov, A. A. 2002, J. Geophys. Res., 107, 1234
Manoharan, P. K., van Driel- Gesztelyi, L., Pick, M., & Démoulin, P. 1996, ApJ, 468, L73
Moreton, G. E. 1960, AJ, 65, 494
Ofman, L. & Thompson, B. J. 2002, ApJ, 574, 440
Podladchikova, O., & Berghmans, D. 2005, Sol. Phys., 228, 265
Shibata, K., Masuda, S., Shimojo, M., Hara, H., Yokoyama, T., Tsuneta, S., Kosugi, T., & Ogawara, Y. 1995, ApJ, 451, L83
Thompson, B. J., Reynolds, B., Aurass, H., Gopalswamy, N., Gurman, J. B., Hudson, H. S., Martin, S. F., & St. Cyr, O. C. 2000a, Sol. Phys., 193, 161
Thompson, B. J., Cliver, E. W., Nitta, N., Delannée, C., & Delaboudinière, J. P. 2000b, Geophys. Res. Letters, 27, 1431
Thompson, B. J., et al. 1999, ApJ, 512, L151
Thompson, B. J., Plunkett, S. P., Gurman, J. B., Newmark, J. S., St. Cyr, O. C., & Michels, D. J. 1998, Geophys. Res. Lett., 25, 2461
Uchida, Y. 1968, Sol. Phys., 4, 30
Wang, Y. M. 2000, ApJ, 543, L89
Warmuth, A., Vršnak, B., Aurass, H., & Hanslmeier, A. 2001, ApJ, 560, L105
Warmuth, A., Vršnak, B., Magdalenic, J., Hanslmeier, A. & Otruba, W. 2004a, A&A, 418, 1101
Warmuth, A., Vršnak, B., Magdalenic, J., Hanslmeier, A. & Otruba, W. 2004b, A&A, 418, 1117
Webb, D. F., Lepping, R. P., Burlaga, L. F., DeForest, C. E., Larson, D. E., Martin, S. F., Plunkett, S. P. & Rust, D. M. 2000, J. Geophys. Res., 105, 27251
Zarro, D. M., Sterling, A. C., Thompson, B. J., Hudson, H. S., & Nitta, N. 1999, ApJ, 520, L139
Zhukov, A. N. & Auchére, F. 2004, A&A, 427, 705